B-nor-methylene Colchicinoid PT-100 Selectively Induces Apoptosis in Multidrug-Resistant Human Cancer Cells via an Intrinsic Pathway in a Caspase-Independent Manner

Andreas Stein, Persefoni Hilken Née Thomopoulou, Corazon Frias, Sina M Hopff, Paloma Varela, Nicola Wilke, Arul Mariappan, Jörg-Martin Neudörfl, Alexey Yu Fedorov, Jay Gopalakrishnan, et al.

ACS OMEGA

http://pubs.acs.org/journal/acsodf

Article

B-nor-methylene Colchicinoid PT-100 Selectively Induces Apoptosis in Multidrug-Resistant Human Cancer Cells via an Intrinsic Pathway in a Caspase-Independent Manner

Andreas Stein,[○] Persefoni Hilken née Thomopoulou,[○] Corazon Frias, Sina M. Hopff, Paloma Varela, Nicola Wilke, Arul Mariappan, Jörg-Martin Neudörfl, Alexey Yu Fedorov, Jay Gopalakrishnan, Benoît Gigant, Aram Prokop,* and Hans-Günther Schmalz*

Cite This: *ACS Omega* 2022, 7, 2591−2603

Read Online

ACCESS | Metrics & More | Article Recommendations | Supporting Information

ABSTRACT: Colchicine, the main active alkaloid from *Colchicum autumnale* L., is a potent tubulin binder and represents an interesting lead structure for the development of potential anticancer chemotherapeutics. We report on the synthesis and investigation of potentially reactive colchicinoids and their surprising biological activities. In particular, the previously undescribed colchicinoid PT-100, a B-ring contracted 6-exo-methylene colchicinoid, exhibits extraordinarily high antiproliferative and apoptosis-inducing effects on various types of cancer cell lines like acute lymphoblastic leukemia (Nalm6), acute myeloid leukemia (HL-60), Burkitt-like lymphoma (BJAB), human melanoma (MelHO), and human breast adenocarcinoma (MCF7) cells at low nanomolar concentrations. Apoptosis induction proved to be especially high in multidrug-resistant Nalm6-derived cancer cell lines, while healthy human leukocytes and hepatocytes were not affected by the concentration range studied. Furthermore, caspase-independent initiation of apoptosis via an intrinsic pathway was observed. PT-100 also shows strong synergistic effects in combination with vincristine on BJAB and Nalm6 cells. Cocrystallization of PT-100 with tubulin dimers revealed its (noncovalent) binding to the colchicine-binding site of β-tubulin at the interface to the α-subunit. A pronounced effect of PT-100 on the cytoskeleton morphology was shown by fluorescence microscopy. While the reactivity of PT-100 as a weak Michael acceptor toward thiols was chemically proven, it remains unclear whether this contributes to the remarkable biological properties of this unusual colchicinoid.

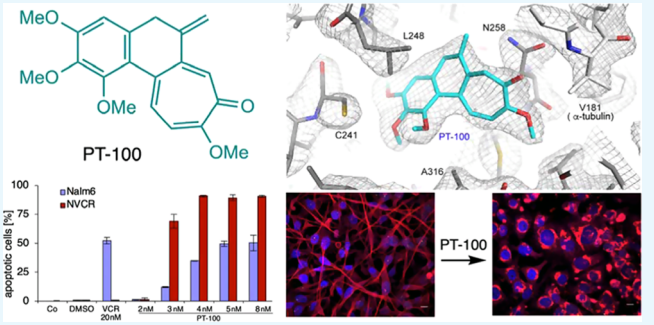

INTRODUCTION

Extracts from the meadow saffron (*Colchicum autumnale* L.) containing the tricyclic alkaloid colchicine (**1**, Figure 1) as the main bioactive component have found use in herbal medicine since ancient times.[1] Colchicine is still used in modern medicine to treat inflammatory diseases like gouty arthritis,[1−4] Behçet's disease,[2,5,6] pericarditis,[2,7,8] and familial Mediterranean fever.[2,9,10] However, the dosage has to be controlled carefully due to a narrow therapeutic window associated with the alkaloid's high systemic toxicity. Thus, overdosing may cause severe side effects ranging from gastrointestinal irritation to death.[2]

Aside from its anti-inflammatory properties, colchicine (**1**) exhibits a strong effect on malignant tumor cells.[11−13] The cytostatic activity of **1** and many of its derivatives is based on the strong binding affinity toward tubulin at the so-called colchicine-binding site (CBS). Tubulins, specifically α-tubulin and β-tubulin, are globular proteins omnipresent in eukaryotic cells.[14] By noncovalent interactions, α,β-heterodimers are formed, which self-assemble into elongated polymer structures (protofilaments) of microtubules. Microtubules are important for the structural integrity and motility of a cell as well as for intracellular transport. In particular, they emanate from the mitotic spindle poles as spindle microtubules and play a central role in accurate cell division during mitosis.[14−16] CBS-binding small molecules like colchicine inhibit the polymerization of α,β-tubulin heterodimers,[17] thus disrupting the microtubule assembly. This causes cell cycle arrest in the G2/M phase and subsequent apoptosis induction in proliferating cells.[18]

Due to the toxicity and high doses required for chemotherapeutic treatment, colchicine (**1**) itself cannot be used in

Received: August 26, 2021
Accepted: December 31, 2021
Published: January 11, 2022

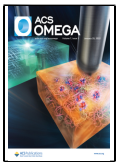

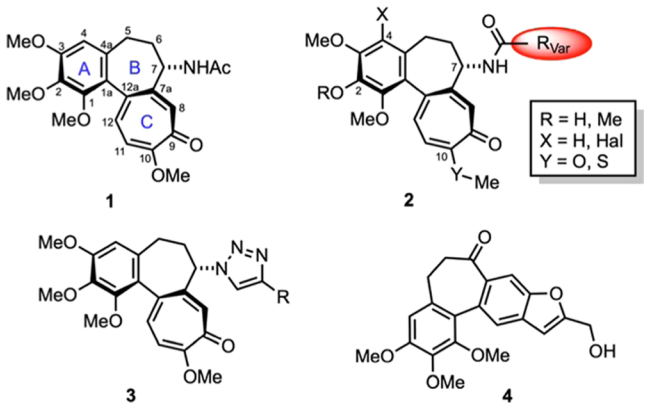

Figure 1. (*aR*,7*S*)-colchicine (**1**) and structures of common colchicine analogues (**2**) and semisynthetic colchicinoids **3** and **4** from our previous work.

cancer therapy.[12] However, the molecule represents a promising lead structure, and countless colchicine-derived compounds of type **2** (compare Figure 1) have been described in the last decades as potential novel chemotherapeutics.[19−22] Contributions from our own laboratories (Figure 1) include triazoles of type **3**[23] and heterocycle-fused allocolchicinoids such as **4**[24−26] exhibiting high activity against relevant cancer cell lines.

While most drugs, including colchicine (**1**), bind reversibly to their protein targets, covalently binding agents (with the exception of a few special compounds such as *β*-lactam antibiotics) have received less attention in pharmacological development due to allegedly higher toxicity risks[27,28] and such compounds have been mainly used for analytical purposes, for instance, in the identification of target proteins of active small molecules.[29−33] In the last decade, however, targeted covalent inhibitors (TCIs) are enjoying increasing attention,[34−37] peaking in the recent development of clinically approved drugs, such as ibrutinib,[38] rociletinib,[39] and afatinib.[39] Like many TCIs,[29,40] these novel anticancer drugs feature an *α*,*β*-unsaturated carbonyl moiety allowing their covalent attachment to a cysteine side chain of the target protein in a Michael-type addition reaction.

In the course of our own research program on novel colchicine-derived compounds, we accidentally recognized that one compound (PT-100), which was initially only obtained as a byproduct, exhibited particularly high cytotoxicity in preliminary screening. This compound was later identified as *exo*-methylene-nor-colchicine **7** (see below), which possibly might act as a covalently binding agent as it represents a potential Michael-like acceptor molecule. Inspired by this observation, we decided to investigate PT-100 (and related colchicine derivatives) in more detail and disclose the results herein.

RESULTS AND DISCUSSION

Chemical Synthesis. We started our investigation with the known conversion of *N*-deacetyl-colchicine (**5**), which is easily obtained from commercially available colchicine in three steps,[41] into Demjanov-rearranged B-nor-colchicine derivative **6** following the protocol of Danieli et al. (Scheme 1).[42] When we tried to react the primary OH function of **6** in a Mitsunobu-type[43] reaction, we observed the formation of elimination product **7**, initially as a byproduct. As this compound exhibited unexpected and promising biological activity (vide infra), we optimized its synthesis. Using a reagent combination of di-*tert*-butyl azodicarboxylate and triphenylphosphine in chloroform (0 °C to room temperature (rt)), the transformation proceeded cleanly, yielding olefin **7** in 84% isolated yield after purification

Scheme 1. Synthesis of 7 and Derivatives Thereof[a]

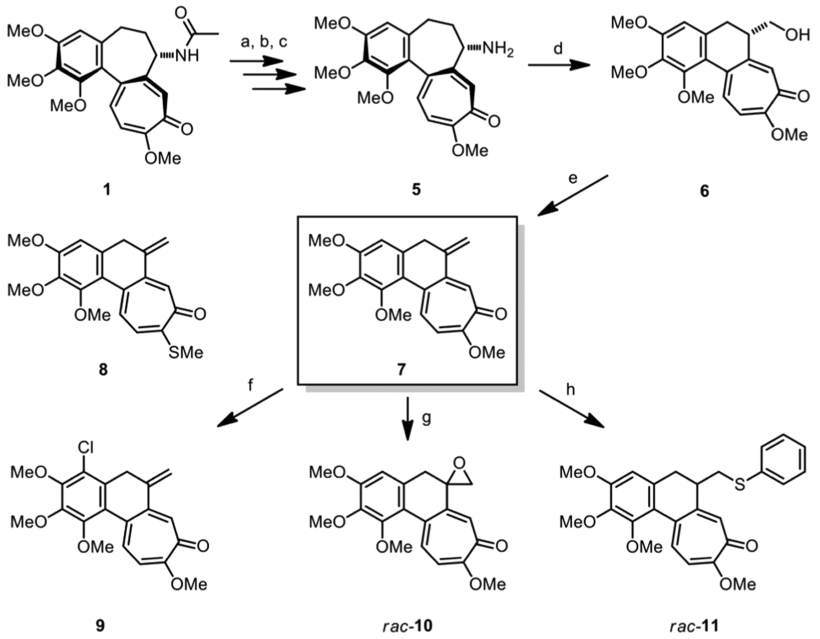

[a]Reagents and conditions: (a) Boc_2O, NEt_3, *N*,*N*-dimethylaminopyridine (DMAP), MeCN, reflux, 6 h, 96%; (b) NaOMe, MeOH, 0 °C, 30 min, rt, 1.5 h, 99%; (c) trifluoroacetic acid (TFA), dichloromethane (DCM), rt, 2 h, 91%; (d) $NaNO_2$, AcOH, H_2O, rt, 5 h, 41%; (e) PPh_3, D^{i}BAD, $CHCl_3$, 0 °C, 1 h, rt, 15 h, 84%; (f) NCS, AcOH, 70 °C, 2.5 h, 45%, (g) DMDO, EtOAc/acetone 1:3, 0 °C, 2 h, rt, 15 h, 34%; (h) PhSH, diisoproylethylamine (DIPEA), MeOH, rt, 2 h, 12%.

https://doi.org/10.1021/acsomega.1c04659
ACS Omega 2022, 7, 2591−2603

A

Comp.	AC_{50} [nM]
1	10 – 20
7	5.0
8	8 – 14
9	≈ 500
rac-**10**	40

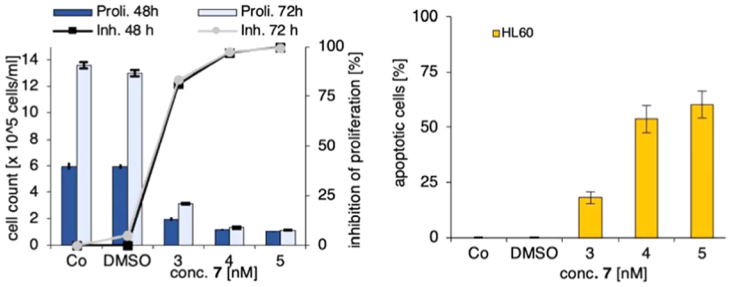

Figure 2. Activity of synthesized colchicinoids. Untreated cells are used as a control (Co). (A) AC_{50} values (concentration at which 50% cells show apoptosis) of compounds **1**, **7**, **8**, **9**, and *rac*-**10** against Nalm6 cells after 72 h incubation (n = 3). (B) Cell proliferation in Burkitt-like lymphoma (BJAB) cells inhibited by **7**. Cells were incubated with different concentrations of **7**. After 48 and 72 h, the cell proliferation was determined using a CASY Cell Counter + Analyzer system. Inhibition of proliferation is given as the percentage of control ± standard deviation (SD) (n = 3). (C) Apoptotic effects in acute myeloid leukemia (AML) cells. HL-60 cells were incubated with different concentrations of **7** for 72 h. Then, DNA fragmentation was measured by flow cytometric analysis. Values are given as the percentage of apoptotic cells ± SD (n = 3).

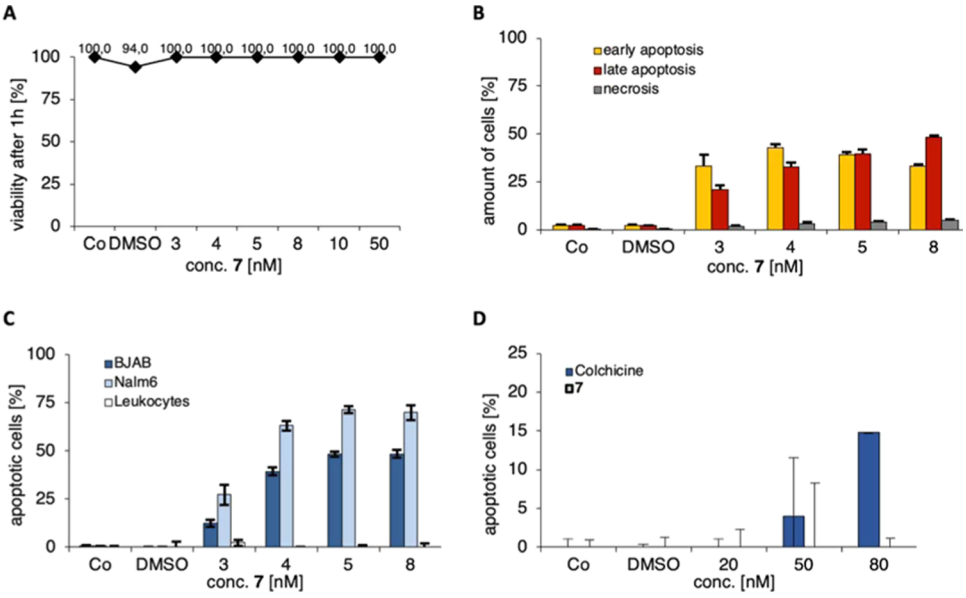

Figure 3. Exclusion of necrosis and proof of selectivity of compound **7** toward cancer cells. Some cells were left untreated as control (Co) or treated only with dimethyl sulfoxide (DMSO). (A) BJAB cells were treated with different concentrations of **7** and incubated for 1 h. Viability was determined by the LDH release assay. Values are given as the percentage of control. (B) Annexin V-FITC/PI assay. BJAB cells were treated with 3−8 nM **7** and incubated for 48 h. The amount of early apoptosis, late apoptosis, and necrosis is shown in percentage. Values are expressed as the percentage of control ± SD (n = 3). (C) Induction of apoptosis in BJAB, Nalm6, and healthy leukocytes. Cells were incubated with **7** at different concentrations. DNA fragmentation was measured after 72 h by flow cytometric analysis. Values are given as the percentage of apoptotic cells based on the total population (n = 3). (D) Healthy human hepatocytes were treated with 20, 50, and 80 nM colchicine or **7** and then incubated for 96 h. DNA fragmentation was measured by flow cytometric analysis. Values are given as the percentage of apoptotic cells and are expressed at means ± SD (n = 3).

on a gram scale. As compound **7** represents a vinylogous Michael acceptor, we decided to also investigate related compounds that might also possibly act as covalently binding agents. Following the protocol of Sun et al.,[44] we prepared the known thiocolchicine analogue **8**. Considering that halogenation at position 4 occasionally has a positive impact on the activity of colchicinoids,[45] we also prepared chlorinated analogue **9** by heating **7** with *N*-chloro succinimide (NCS) in acetic acid. In addition, we succeeded in synthesizing *rac*-**10** by epoxidation of **7** with dimethyldioxirane (DMDO).

To probe whether compound **7** is able to react as a Michael acceptor with S nucleophiles, it was treated with thiophenol in the presence of a base to indeed afford adduct *rac*-**11** (Scheme 1). Other thiols, such as N-Boc-cysteamine, N-Boc-cysteine methyl ester, and 2-phthalimido ethanethiol, were found to also react with **7**; however, complex mixtures of air and/or light-sensitive products were formed in these cases. Mass spectrometry of the crude mixtures indicated the formation of the expected adducts associated with the disappearance of the olefinic protons in the ^{1}H NMR spectra.

Biological Investigations. Initial biological experiments using B-cell precursor leukemia cell cultures (Nalm6) showed that compound **7** (and to a slightly lower extend also *rac*-**10**) exhibits remarkable cytotoxic activity. Compound **7** is about 100 times more active than the chlorinated derivative **9** and twice as active as thio analogue **8** (Figure 2A). Compound **7** was therefore selected for further in-depth investigations.

We found that low nanomolar concentrations of **7** (IC_{50} < 3 nM) are sufficient to effectively inhibit the growth of quickly proliferating Burkitt-like lymphoma (BJAB) cells (Figure 2B). Increasing the concentration from 3 to 8 nM led to a complete (up to 100%) inhibition of cell proliferation. Noteworthy, **7** also

https://doi.org/10.1021/acsomega.1c04659
ACS Omega 2022, 7, 2591−2603

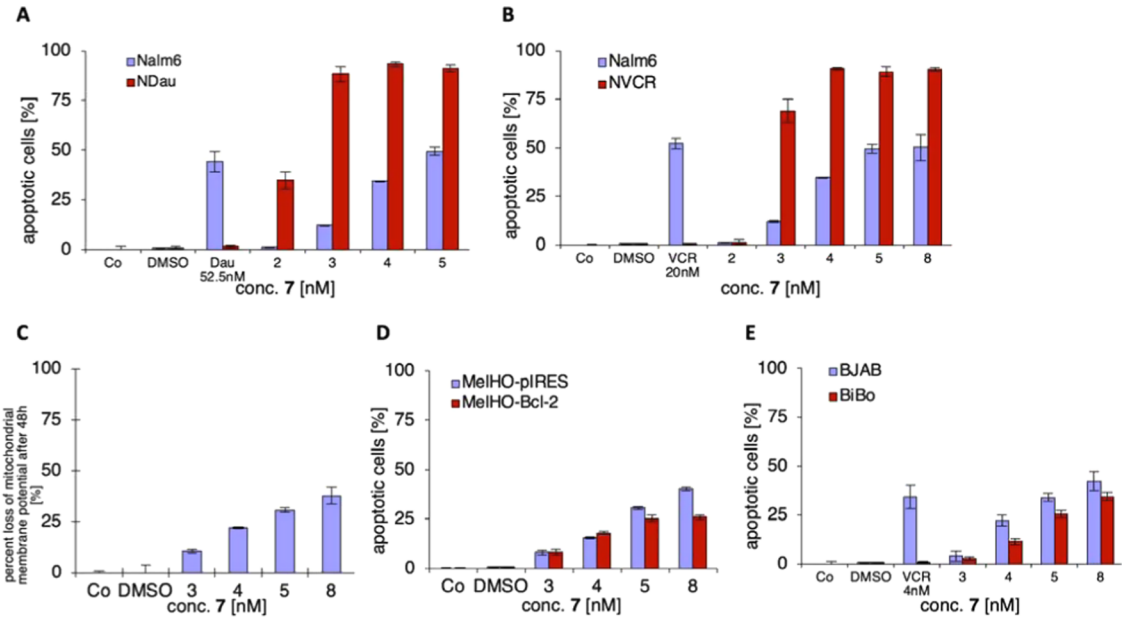

Figure 4. Investigation of the mechanism of action of 7. Control (Co) cells were left untreated. (A, B) Induction of apoptosis in Nalm6, NDau, and NVCR cells. Cells were incubated with 7 at different concentrations. To prove the resistance, cells were additionally treated with vincristine (VCR) at 20 nM or daunorubicin (Dau) at 52.5 nM, respectively. Apoptosis induction was determined by DNA fragmentation, measured after 72 h by flow cytometric analysis. The values are given as the percentage of apoptotic cells based on the total population ± SD (n = 3). (C) Loss of mitochondrial membrane potential. After treatment of BJAB cells with different concentrations of 7 and incubation for 48 h, mitochondrial membrane permeability was measured by flow cytometric analysis after staining with JC-1 dye. Values are given as the percentage of cells with low $\Delta\Psi_m$ ± SD (n = 3). (D) MelHO-pIRES and MelHO-Bcl-2 cells were treated with different concentrations of 7. The incubation time was 72 h. DNA fragmentation was measured by flow cytometric analysis of the cellular DNA content. Values are given as the percentage of apoptotic cells and are expressed as means ± SD (n = 3). (E) Effect of 7 on vincristine-resistant (BiBo) and normal BJAB cells. As a control, both cell lines were treated with 4 nM vincristine (VCR). The incubation time was 72 h. DNA fragmentation was measured by flow cytometric analysis of cellular DNA content. Values are given as the percentage of apoptotic cells and are expressed as means ± SD (n = 3).

induces high levels of apoptosis in the AML cell line HL-60 already at low nanomolar concentrations (Figure 2C).

Apoptosis and necrosis are two different types of cell death.[54] The lactate dehydrogenase (LDH) assay confirmed that the cytotoxic effects of 7 result in apoptosis and not necrosis.[55] After incubating BJAB cells for 1 h with 3−50 nM 7, we measured the LDH release into the culture medium by enzyme-linked immunosorbent assay (ELISA). At all concentrations, the viability of the cells stayed at 100% (Figure 3A). The Annexin V fluorescein isothiocyanate/propidium iodide (V-FITC/PI) assay showed early apoptosis values between 33.2 and 42.6% at 3−8 nM 7 (Figure 3B). A significant increase of late apoptosis was detected at higher concentrations of 7. In accordance with the results of the LDH assay, no significant levels of necrosis were detected. Remarkably, compound 7 was found to be highly selective toward the tumor cells tested, while it showed no toxicity against healthy leukocytes (Figure 3C). Even at increased concentrations of 7 (up to 8 nM), at which BJAB lymphoma and Nalm6 leukemia cells show high levels of apoptosis, leukocytes remained virtually unaffected. Furthermore, hepatotoxicity at relevant concentrations of 7 could be excluded. We tested the substance at concentrations of up to 80 nM on healthy human hepatocytes without any loss of vitality. In comparison, we observed that human hepatocytes are affected by colchicine at these concentrations (Figure 3D).

Finding substances that overcome resistance in tumor cell lines is a particular challenge in oncology research because failure in chemotherapy mainly results from cellular drug resistance.[46,47] Therefore, the fact that 7 preferably induces apoptosis in vincristine-resistant (NVCR) and daunorubicin-resistant (NDau) Nalm6 cells represents a remarkable discovery. These cells are multidrug-resistant (MDR) due to the overexpression of the drug efflux pump P-glycoprotein (P-gp) encoded by the MDR1/ABCB1 gene and are resistant against, among other drugs, fludarabine, paclitaxel, and colchicine.[48−50] P-gp overexpression is the most common mechanism of MDR and causes a decrease of intracellular drug concentration.[51,52] While normal Nalm6 cells are only slightly affected by 7 at low concentrations (3−4 nM), the corresponding fully vincristine-resistant cell line (NVCR) already displays ≥90% apoptosis induction at 4 nM (Figure 4B). A similar effect was found for daunorubicine-resistant Nalm6 (NDau) cells (Figure 4A). Cytostatic agents like vincristine, daunorubicin, and paclitaxel attach to the transmembrane domains of P-gp, but 7 has the potential to overcome the binding position in an impressive way.[52,53]

The two main pathways to introduce apoptosis are the mitochondria-dependent intrinsic pathway and the death receptor-dependent extrinsic pathway.[57] The result of both pathways is the activation of caspases that regulate apoptosis.[58] A protein of the mitochondrial pathway is the strong antiapoptotic protein Bcl-2 that is overexpressed in several tumor cell lines. Aside from the fact that common cytostatic drugs are often caspase-3 (C3)-dependent, they usually cannot address Bcl-2 overexpressing cancer cells.[64] To clarify the possible interplay of 7 with Bcl-2, we used two different cell lines and their modified variants that are characterized by Bcl-2 overexpression. While the melanoma cell line MelHO-pIRES is just transfected with the pIRES plasmid, the MelHO-Bcl-2 cells also contain Bcl-2 cDNA within pIRES. This results in a 30-fold

https://doi.org/10.1021/acsomega.1c04659
ACS Omega 2022, 7, 2591−2603

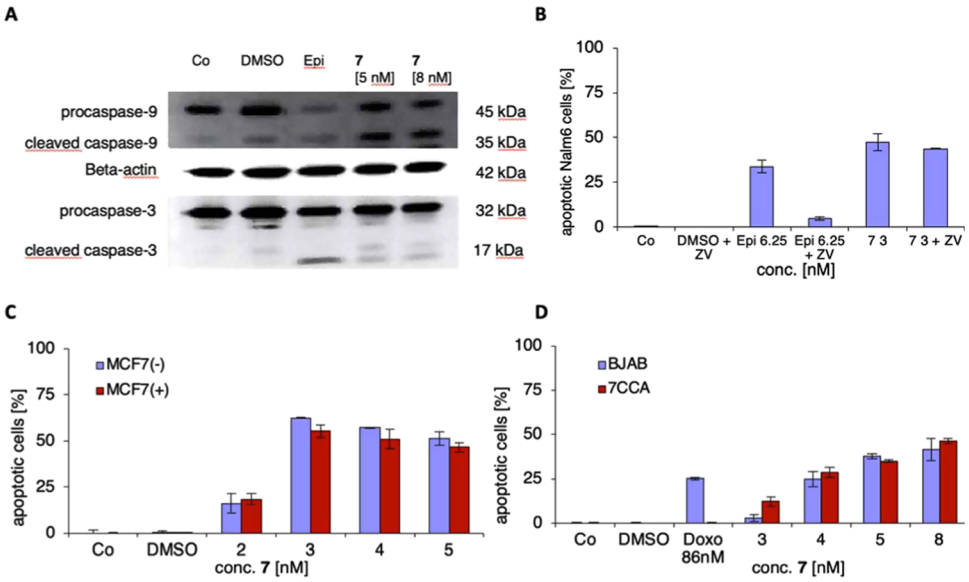

Figure 5. Compound 7 induces apoptosis via the intrinsic pathway in a caspase-independent fashion. As a control, some cells were left untreated (Co). (A) Procaspase-3 and procaspase-9 processing. BJAB cells were incubated with 5 and 8 nM 7. Epirubicin (Epi) was used as the positive control. Sodium dodecyl sulfate-polyacrylamide gel electrophoresis (SDS-PAGE) was used for separation of 20 μg of cytosolic proteins followed by western blot analysis. Immunoblotting was done with anti-C3 and anti-C9 antibodies. Loading and blotting control via β-actin. (B) Experimental proof of caspase independence by treatment of Nalm6 cells with 3 nM 7 alone and in combination with pancaspase inhibitor ZVAD-fmk (ZV). As a control, 6.25 nM epirubicin (Epi) was added alone and in combination with ZV. After 72 h of incubation, DNA fragmentation was measured by flow cytometric analysis using three batches per concentration. Values are given as the percentage of apoptotic cells ± SD. (C) C3-independent activity of 7 shown by treatment of MCF7(−) cells and MCF7(+) cells with different concentrations of 7. DNA fragmentation was measured after 72 h by flow cytometric analysis of cellular DNA content (staining with JC-1 dye). Values are given as the percentage of cells with hypodiploid DNA ± SD (n = 3). (D) Second proof of C3-independent action of 7. BJAB and doxorubicin-resistant 7CCA cells were treated with different concentrations of 7. Doxorubicin (Doxo) was added to both cell lines (c = 86 nM) to prove the resistance. DNA fragmentation was measured after 72 h by flow cytometric analysis of the cellular DNA content. Values are given as the percentage of cells with hypodiploid DNA ± SD (n = 3).

overexpression of Bcl-2 in the MelHO-Bcl-2 cell line compared to MelHO-pIRES. Figure 4D shows that at lower concentrations of 7 (3 and 4 nM) the apoptotic effects in both MelHO cell lines are similar. With increasing concentrations of 7, a stronger apoptotic effect is observed for the MelHO-pIRES cells (up to 40% apoptotic cells) as compared to the MelHO-Bcl-2 cells (up to 25%). As expected, Bcl-2 overexpression leads to a suppression of apoptosis; however, compound 7 is powerful enough to still induce apoptosis in MelHO-Bcl-2 cells to a significant extent.

The second resistant BJAB cell line that we generated in our lab (named BiBo) is characterized by vincristine resistance. The resistance mechanism is also based on Bcl-2 overexpression. As expected, DNA fragmentation upon treatment of BJAB and BiBo cells with 7 results in pronounced apoptosis induction in both cell lines (Figure 4E). Nevertheless, the effect in BiBo cells is around 10% lower than that in the BJAB cells for the same reasons explained above.

The intrinsic pathway is associated with the loss of the mitochondrial membrane potential and associated changes in its permeability.[59,60] Furthermore, caspase-9 participates as an initiator and caspase-3 as another key component in the mitochondrial pathway.[61,62] Western blot analysis after incubating BJAB cells with 5 and 8 nM 7 for 36 h revealed activation of caspase-9 (C9) but no significant activation of caspase-3 (C3) (Figure 5A). This indicates the involvement of the intrinsic pathway in the induction of apoptosis by 7 as reflected by the appearance of cleaved C9 and small consumption of procaspase-3. The induction of apoptosis by 7 via the intrinsic mitochondrial pathway is also confirmed by the dose-dependent loss of the mitochondrial membrane potential of BJAB cells (Figure 4C). At 5 nM concentration, 7 leads to disruption of the membrane potential of 30% cells (increasing to 38% at 8 nM).

Interestingly, 7 also induced DNA fragmentation in the C3 defective human breast cancer cell line MCF7(−) as well as in the modified strain MCF7(+), which is able to express C3 (Figure 5C). This protease exerts a key function in both the intrinsic and extrinsic pathways.[61] Accordingly, most of the common cytostatic agents induce apoptosis in a C3-dependent manner.[63] C3 independence of 7 was further underlined by testing the substance against regular BJAB as well as doxorubicin-resistant BJAB (7CCA) cells, the latter being characterized by downregulation of C3 expression. The fact that the percentage of apoptotic cells was as high or even higher in the treated 7CCA cells as compared to the BJAB cells again indicates C3-independent induction of apoptosis by 7 (Figure 5D).

Remarkably, we also found out that the strong proapoptotic effect of 7 in Nalm6 cells cannot be blocked by pancaspase inhibitor zVAD-fmk. For this experiment, Nalm6 cells were incubated with 7 alone and with a combination of 7 and zVAD-fmk, respectively, and the percentage of apoptotic cells was determined by FACScan analysis. The results shown in Figure 5B clearly indicate that 7 induces apoptosis not only independently from C3 but also from the general caspase cascade, despite the activation of C9 (Figure 5A).

The combination of two cytostatic drugs represents a well-explored strategy to reach a better therapeutic response due to sensitization of the tumor cells.[56] To test the synergistic effects

https://doi.org/10.1021/acsomega.1c04659
ACS Omega 2022, 7, 2591−2603

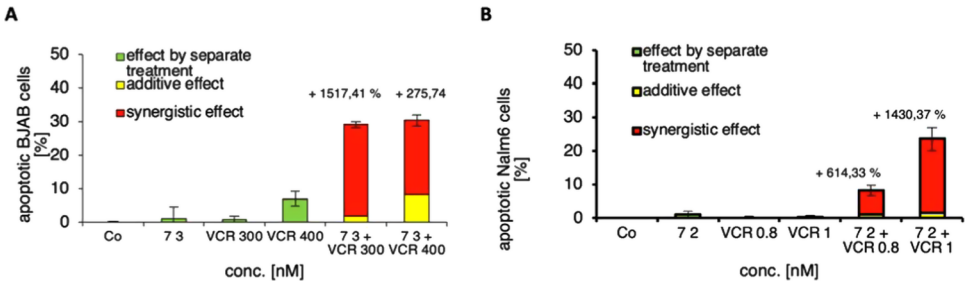

Figure 6. Synergistic effects of 7 and vincristine. Cells were treated with different concentrations of 7 and vincristine, either separately or in combination. Control cells were left untreated. After 72 h of incubation, DNA fragmentation was measured by flow cytometric analysis using three batches per concentration. Values are given as the percentage of apoptotic cells ± SD. The synergistic effect in percentage is written above. (A) BJAB cells were treated with 7 (3 nM) and vincristine (0.3 and 0.4 μM). (B) Nalm6 cells were treated with 7 (2 nM) and vincristine (0.8 and 1 nM).

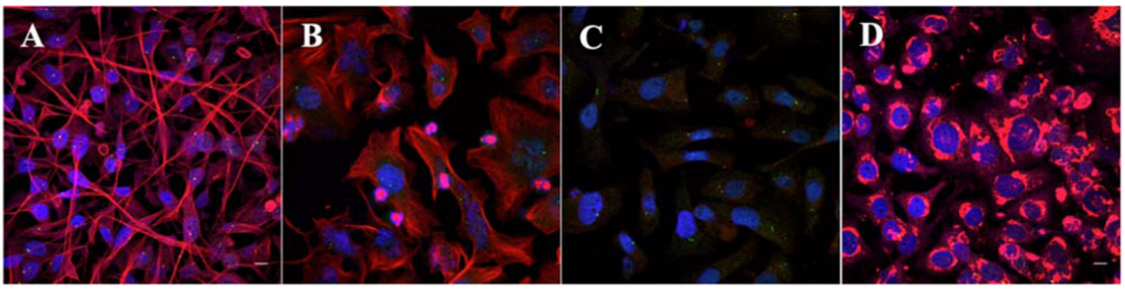

Figure 7. Microtubule morphology of MDA-MB-231 breast cancer cells after 24 h incubation. Microtubules (red) and centrosomes (green) were stained with antibodies, while 4,6-diamidino-2-phenylindole (DAPI) was used to visualize DNA (blue). The white scale bars correspond to a distance of 10 μm. (A) Control (untreated cells), (B) paclitaxel (100 nM), (C) colchicine (**1**) (100 nM), and (D) 7 (100 nM).

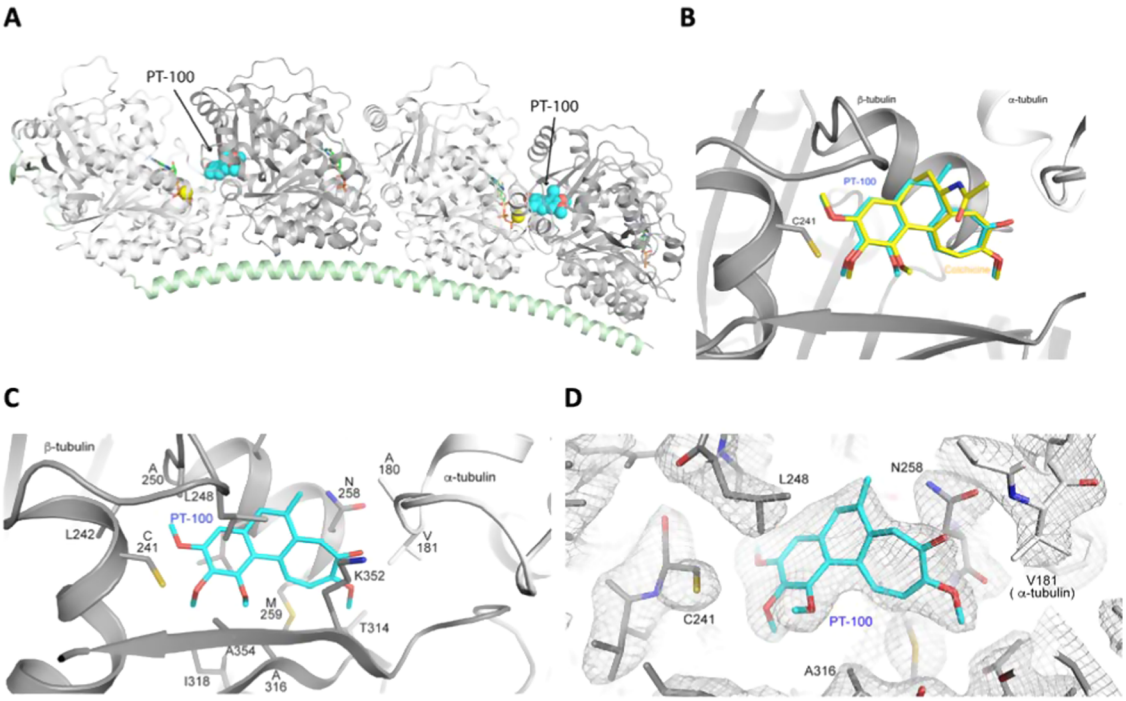

Figure 8. X-ray crystal structure of 7 (PT-100, cyan) bound to tubulin. (A) View at the whole T_2R complex comprising two α,β-tubulin heterodimers (in gray, with the β-subunit in darker gray) stabilized by the stathmin-like domain of the RB3 protein (green) and 7 binding to β-tubulin at the interface with the α-subunit. (B) Comparison of the binding geometries of PT-100 (7, cyan) and colchicine (**1**, yellow, from PBD ID 5EYP).[65] The β-tubulin subunits have been superimposed; only tubulin with bound PT-100 is shown. (C) Close-up perspective of 7 occupying the colchicine-binding site. (D) Same perspective showing the 2 $F_{obs} - F_{calc}$ electron density map contoured at the 1 σ level.

of 7, we combined this substance at very low concentrations with vincristine. Separate treatment of BJAB cells with either 7 (3 nM) or vincristine (0.3 and 0.4 μM) showed no significant apoptosis induction after 72 h. However, the combined effect of 7 and vincristine at the same concentrations resulted in significantly higher values than the sum of their individual parts (Figure 6A). The highest synergistic effect (factor 15) is observed at a concentration of 3 nM 7 and 0.3 μM vincristine. In

https://doi.org/10.1021/acsomega.1c04659
ACS Omega 2022, 7, 2591−2603

a similar fashion, Nalm6 cells were treated with 7 (2 nM) and vincristine (0.8 and 1 nM) again, resulting in a strong (up to 14 fold) synergistic effect (Figure 6B). These strong synergistic effects indicate that 7 has the potential to effectively sensitize leukemia and lymphoma cells toward vincristine.

In addition to the cytotoxicity studies, the effect of 7 on microtubule cytoskeleton morphology of MDA-MB-231 breast cancer cells was explored by means of immunofluorescence microscopy.[23] For this purpose, cells were incubated with 7 at a concentration of 100 nM and microtubules, centrosomes, and DNA were visualized using respective antibodies such as anti-tubulin and anti-Cep152 (Figure 7). While untreated cells (Figure 7A) showed a typical microtubule network, incubation with 100 nM paclitaxel as a microtubule-stabilizing agent resulted in the formation of stable microtubules (Figure 7B). In the case of colchicine (**1**), the microtubule network collapsed completely (Figure 7C). Interestingly, compound 7 also suppressed the formation of the microtubule network (at 100 nM), however, short microtubule fragments tending to localize around the cell nucleus were observed (Figure 7D).

X-ray Crystallography. To confirm that the remarkable bioactivity of 7 (PT-100) indeed results from its binding to the CBS of tubulin and to probe whether it possibly attaches there in a covalent fashion, we performed an X-ray crystal structure analysis of a complex of 7 with stathmin-stabilized tubulin heterodimers (Figure 8).[17] The structure confirms that 7 binds to the colchicine-binding site in a similar fashion to colchicine. The long distance (approx. 9 Å) between the (potentially reactive) methylene group of 7 and the nearest nucleophilic amino acid residue (Cys241, Figure 8C) indicates that the formation of a covalent bond between 7 and tubulin is highly unlikely to occur, at least not in the experimentally observed binding mode.

SUMMARY AND CONCLUSIONS

The novel colchicine analogue PT-100 (7), which is readily prepared in a few chemical steps, from the natural product colchicine was identified as a highly potent cytotoxic agent against several relevant tumor cell lines. Compound 7 was found to exhibit apoptotic and antiproliferative effects at very low (nanomolar) concentrations in the acute lymphoblastic leukemia cell line Nalm6, the acute myeloid leukemia cell line HL-60, as well as different cell lines from solid tumors such as the Burkitt-like lymphoma (BJAB), human breast cancer (MCF7), and melanoma (MelHO). As an outstanding feature, 7 was shown to overcome multiple resistances in both leukemia and lymphoma cells. Extremely high activities were observed in vincristine- and daunorubicin-resistant Nalm6 cells in comparison to nonresistant Nalm6 cells. Doxorubicin- and vincristine-resistant BJAB cells were also strongly affected. For Nalm6 and BJAB cells, a pronounced synergetic (sensitizing) effect (up to 15-fold) in combination with vincristine was observed. As another noteworthy property, we found that 7 initiates apoptosis through a caspase-independent pathway by investigating apoptosis induction in the presence of pancaspase inhibitor ZVAD and by studying caspase-3 underexpressing cells. Although 7 was able to induce apoptosis in a caspase-independent manner, it still had the potential to activate caspases 9 and 3 as shown by western blot analysis. These results indicated the involvement of the intrinsic pathway of apoptosis in accordance with the loss of mitochondrial membrane potential. The high anticancer potential of 7 was further demonstrated by its activity against Bcl-2 overexpressing BiBo and MelHO-Bcl-2 cells, overcoming the strong antiapoptotic character of these cells that are not affected by most other cytostatic drugs. The cell biological investigations were complemented by demonstrating the strong effect of 7 on the cytoskeleton morphology of MDA-MB-231 cells. Finally, an X-ray crystal structure of 7 bound to the α,β-tubulin dimer confirmed its canonical binding to the colchicine-binding site.

All in all, PT-100 (7) represents a promising anticancer substance for future investigation because it shows high selectivity toward tumor cells and does not induce apoptosis in healthy human leukocytes. A further very important fact is that the substance appears not to be hepatotoxic. Toxicity is a major problem for colchicine (**1**) and prevents its clinical use in tumor therapy.[20] The comparison of 7 and **1** in human hepatocytes underlines the hepatotoxicity of **1**, whereas 7 does not influence the cells.

EXPERIMENTAL SECTION

Chemistry. *General Information.* All moisture-sensitive reactions were carried out under an argon atmosphere using Schlenk flasks and needle/syringe techniques. Glassware was flame-dried under vacuum and flushed with argon once cooled down to room temperature. Syringes and needles were flushed with argon directly prior to use. NMR spectra were recorded on Bruker AV 300, 400, 500, and 600 instruments. Chemical shifts (δ) are given in ppm relative to the solvent reference as an internal standard ($CDCl_3$, δ (^{1}H): 7.24 ppm, δ (^{13}C): 77.0 ppm). Signal multiplicity is indicated as follows: s for singlet, d for doublet, dd for doublet of doublets, t for triplet, m for multiplet, and so on. Coupling constants, if applicable, are given as J in hertz. For atom assignment (elucidated by heteronuclear multiple bond coherence (HMBC), heteronuclear multiple quantum coherence (HMQC) and H,H-COSY/H,H-NOESY experiments), see the Supporting Information. High-resolution mass spectra (HRMS) were recorded on a Thermo Fisher LTQ Orbitrap XL—FTMS analyzer (HRMS-ESI). Fourier transform infrared (FT-IR) spectra were recorded on a PerkinElmer FT-IR Spectrum Two spectrometer. Absorption bands are given in wavenumbers ($\tilde{\nu}$, cm^{-1}) and are characterized for their relative intensity (w for weak, m for medium, s for strong, and vs for very strong). Melting points (mp) were measured on a Büchi B-545 melting point apparatus and are uncorrected. Optical rotation $[\alpha]$ was measured on an Anton Paar polarimeter MCP 200 at 20 °C and λ = 589 or 546 nm (cuvette length, 0.5 dm; volume, 1.0 mL). The concentration is given in g/100 mL. Flash chromatography was performed using silica gel for chromatography supplied by Acros (0.035−0.070 mm, 60 Å). Thin-layer chromatography (TLC) plates (Merck silica gel 60 F254) were used to monitor reaction progress, and spots were visualized using a 254 nm UV lamp. Chemicals and solvents for synthesis were purchased from common suppliers and used without further purification. Starting material *N*-deacetylcolchicine (**5**) was prepared by well-established methodologies.[66] Alcohol **6** was then synthesized following a modified and scaled-up literature procedure.[67]

*(S)-6-(Hydroxymethyl)-1,2,3,9-tetramethoxy-5,6-dihydro-8H-cyclohepta[a]naphthalen-8-one (**6**).* In a 100 mL round-bottom flask was dissolved 1.20 g (3.33 mmol) of *N*-deacetylcolchicine (**5**) in 45 mL of H_2O before 345 mg (5.00 mmol) of sodium nitrite and 0.48 mL (500 mg, 8.33 mmol) of acetic acid were added (color change from yellow to orange). The reaction mixture was stirred at room temperature for 5 h and then extracted four times with CH_2Cl_2. The combined

https://doi.org/10.1021/acsomega.1c04659
ACS Omega 2022, 7, 2591−2603

organic layers were washed with saturated aqueous $NaHCO_3$, dried over $MgSO_4$, and concentrated under reduced pressure. The crude product was purified by column chromatography (CH_2Cl_2/MeOH, 14:1) to yield 645 mg (1.80 mmol, 54%) of product **6** as yellow foam. ^{1}H NMR (300 MHz, $CDCl_3$): δ [ppm] = 2.90−2.96 (m, 2H), 2.97−3.08 (m, 1H), 3.36−3.47 (m, 1H), 3.55−3.65 (m, 1H), 3.68 (s, 3H), 3.91 (s, 6H), 3.99 (s, 3H), 6.59 (s, 1H), 6.82 (d, $^3J_{H,H}$ = 11.0 Hz, 1H), 7.36 (s, 1H), 7.93 (d, $^3J_{H,H}$ = 11.0 Hz, 1H). ^{13}C NMR (75 MHz, $CDCl_3$): δ [ppm] = 30.4, 47.1, 55.9, 56.2, 61.1, 63.3, 107.6, 112.8, 121.2, 132.3, 132.4, 133.1, 136.9, 141.7, 149.1, 151.8, 153.4, 163.4, 179.2. HRMS (ESI): calcd for $[M + Na]^+$ ($C_{20}H_{22}NaO_6$): 381.13086; found: 381.13052. FT-IR (ATR): $\tilde{\nu}$ [cm^{-1}] = 3394 (br, m), 1609 (m), 1250 (s), mp: 176 °C [Lit:[67] 174 °C]. $[\alpha]_{589}$ = +20.2°, $[\alpha]_{546}$ = +41.2° ($CHCl_3$, c = 1.01). R_f = 0.19 (CH_2Cl_2/MeOH, 14:1).

*1,2,3,9-Tetramethoxy-6-methylen-5,6-dihydro-8H-cyclohepta[a]naphthalen-8-one (**7**).* Under an argon atmosphere, a solution of 645 mg (1.8 mmol) **6** in 15 mL of dry chloroform was cooled to 0 °C. About 708 mg (2.7 mmol) of PPh_3 and 580 mg (2.52 mmol) of di-*tert*-butyl azodicarboxylate (D^tBAD) were added, and the reaction mixture was stirred at 0 °C for 1 h. After warming to rt, stirring was continued overnight. TLC control indicated total conversion. The solvent was removed under reduced pressure, and the crude product was purified by flash column chromatography (silica, CyHex/EtOAc/EtOH 4:1:1). In total, 517 mg (1.52 mmol, 84%) of product **7** was obtained as bright yellow foam. ^{1}H NMR (300 MHz, $CDCl_3$): δ [ppm] = 3.44 (s, 2H), 3.69 (s, 3H), 3.91 (s, 6H), 4.00 (s, 3H), 5.20 (s, 1H), 5.49 (s, 1H), 6.58 (s, 1H), 6.84 (d, $^3J_{H,H}$ = 10.9 Hz, 1H), 7.59 (s, 1H), 7.96 (d, $^3J_{H,H}$ = 10.9 Hz, 1H). ^{13}C NMR (75 MHz, $CDCl_3$): δ [ppm] = 38.9, 56.0, 56.2, 61.0, 61.1, 105.9, 112.5, 113.8, 121.7, 132.0, 132.7, 132.8, 133.6, 141.7, 145.5, 146.9, 151.9, 153.3, 163.2, 179.7. HRMS (ESI): calcd for $[M + H]^+$ ($C_{20}H_{21}O_5$): 341.13835; found: 341.13826. FT-IR (ATR): $\tilde{\nu}$ [cm^{-1}] = 1581 (s), 1555 (s), 1383 (s), 1330 (s), 1242 (s), 1084 (s). Mp: 168 °C. R_f = 0.25 (CyHex/EtOAc/EtOH, 4:1:1).

*4-Chloro-1,2,3,9-tetramethoxy-6-methylen-5,6-dihydro-8H-cyclohepta[a]naphthalen-8-one (**9**).* Under an inert atmosphere were dissolved 80.0 mg (0.23 mmol) of olefin **7** and 47.0 mg (0.35 mmol) of NCS in 1.40 mL of HOAc and heated up to 70 °C for 5 h. The reaction mixture was then cooled to 0 °C and treated with a saturated aqueous solution of $Na_2S_2O_3$ and a saturated aqueous solution of $NaHCO_3$ (*attention:* strong evolution of gas). The aqueous layer was extracted three times with $CHCl_3$, and the combined organic layers were dried over $MgSO_4$, filtered, and concentrated under reduced pressure. The crude product was purified by column chromatography (CyHex/EtOAc/EtOH, 6:1:1) to yield 40.0 mg (0.11 mmol, 45%) of product **9** as a yellow oil. ^{1}H NMR (600 MHz, $CDCl_3$): δ [ppm] = 3.58 (s, 2H), 3.64 (s, 3H), 3.95 (s, 3H), 3.96 (s, 3H), 4.00 (s, 3H), 5.26 (s, 1H), 5.53 (s, 1H), 6.81 (d, $^3J_{H,H}$ = 10.9 Hz, 1H), 7.57 (s, 1H), 7.90 (d, $^3J_{H,H}$ = 10.9 Hz, 1H). ^{13}C NMR (150 MHz, $CDCl_3$): δ [ppm] = 38.1, 56.3, 60.2, 61.3, 61.4, 112.0, 115.1, 121.2, 126.0, 131.4, 131.8, 132.4, 133.3, 144.3, 146.6, 146.7, 149.9, 150.6, 163.9, 179.7. HRMS (ESI): calcd for $[M + Na]^+$ ($C_{20}H_{19}ClNaO_5$): 397.08132; found: 397.08139. FT-IR (ATR): $\tilde{\nu}$ [cm^{-1}] = 1711 (s), 1584 (s), 1462 (s), 1385 (s), 1255 (s). R_f = 0.19 (CyHex/EtOAc/EtOH, 6:1:1).

*(RS)-1,2,3,9-Tetramethoxyspiro[cyclohepta[a]-naphthalene-6,2′-oxiran]-8(5H)-one (rac-**10**).* To a solution of 102 mg (0.3 mmol, 1.0 equiv) of olefin **7** and 1.00 g (12.0 mmol) of $NaHCO_3$ in 7 mL of 4:2:1 H_2O/EtOAc/acetone was added 369 mg (1.2 mmol) of oxone at 0 °C. After 30 min, another 553 mg (1.8 mmol) of oxone was added. Stirring was continued for 30 min before the last portion of 922 mg (3.0 mmol) of oxone was added. The reaction mixture was stirred for 1 h at 0 °C, before TLC indicated almost full conversion. Reactive species were quenched by addition of 10% w/v aqueous sodium pyrosulphite solution, and the reaction mixture was extracted three times with methylene chloride. The combined organic extracts were dried over magnesium sulfate, and volatiles were removed under reduced pressure. The crude product required multiple purification steps by flash column chromatography (silica, Cy/EtOAc/EtOH 6:1:1), giving 43 mg (0.12 mmol, 40%) of *rac*-**10** as yellow foam. ^{1}H NMR (300 MHz, $CDCl_3$): δ [ppm] = 2.36 (d, $J_{H,H}$ = 14.6 Hz, 1H), 2.74 (dd, $J_{H,H}$ = 5.5, 1.7 Hz; 1H), 2.92 (d, $J_{H,H}$ = 5.5 Hz, 1H), 3.39 (dt, $J_{H,H}$ = 14.4, 1.2 Hz; 1H), 3.73 (s, 3H), 3.91 (s, 3H), 3.92 (s, 3H), 3.99 (s, 3H), 6.54 (s, 1H), 6.81 (d, $^3J_{H,H}$ = 11.1 Hz, 1H), 7.39 (s, 1H), 7.94 (d, $^3J_{H,H}$ = 10.9 Hz, 1H). ^{13}C NMR (75 MHz, $CDCl_3$): δ [ppm] = 36.8, 56.0, 56.2, 57.3, 58.4, 61.1, 106.9, 112.3, 121.2, 129.3, 131.0, 132.4, 133.2, 142.1, 146.1, 151.9, 153.4, 163.4, 179.8. HRMS (ESI): calcd for $[M + Na]^+$ ($C_{20}H_{20}NaO_6$): 379.11521; found: 379.11551. FT-IR (ATR): $\tilde{\nu}$ [cm^{-1}] = 1618 (m), 1248 (s), 1085 (s). Mp: 112−115 °C. R_f: 0.18 (CyHex/EtOAc/EtOH, 6:1:1).

*(RS)-1,2,3,9-Tetramethoxy-6-((phenylthio)methyl)-5H-cyclohepta[a]naphthalen-8(6H)-one (rac-**11**).* A solution of 68 mg (0.2 mmol) of olefin **7** and 20 μL (24 mg, 0.22 mmol) of thiophenol in dry methanol (1 mL) was cooled to 0 °C. About 40 μL (28 mg, 0.22 mmol) of DIPEA was added, and the reaction was stirred for 6 h, until TLC indicated full conversion. The solvent was removed *in vacuo*. The residue was subjected to column chromatography separation (silica, Cy/EtOAc/EtOH 10:1:1 to 4:1:1), yielding 11 mg (0.024 mmol, 12%) of adduct *rac*-**11**. ^{1}H NMR (500 MHz, $CDCl_3$): δ [ppm] = 2.62 (dd, $J_{H,H}$ = 13.7, 10.9 Hz; 1H), 2.84 (dd, $J_{H,H}$ = 15.0, 4.3 Hz; 1H), 2.92−297 (m, 1H), 3.05 (dd, $J_{H,H}$ = 13.7, 4.7 Hz; 1H), 3.14 (dd, $J_{H,H}$ = 15.1, 2.2 Hz; 1H), 3.69 (s, 3H), 3.90 (s, 3H), 3.92 (s, 3H), 9.98 (s, 3H), 6.55 (s, 1H), 6.81 (d, $^3J_{H,H}$ = 11.1 Hz, 1H), 7.22 (t, $^3J_{H,H}$ = 7.2 Hz, 1H), 7.24 (s, 1H), 7.31 (t, $^3J_{H,H}$ = 8.2 Hz, 2H), 7.36 (d, $^3J_{H,H}$ = 7.1 Hz, 2H), 7.94 (d, $^3J_{H,H}$ = 11.0 Hz, 1H). ^{13}C NMR (75 MHz, $CDCl_3$): δ [ppm] = 31.8, 36.5, 43.8, 56.0, 56.3, 61.1, 61.2, 108.2, 112.6, 121.2, 126.7, 129.2, 130.1, 131.6, 132.5, 132.5, 135.0, 136.5, 141.8, 150.6, 151.9, 153.5, 163.6, 179.3. HRMS (ESI): calcd for $[M + Na]^+$ ($C_{26}H_{26}NaO_5S$): 473.13932; found: 473.13916. FT-IR (ATR): $\tilde{\nu}$ [cm^{-1}] = 1585 (m), 1251 (s), 1137 (s), 1086 (s). Mp: 75−76 °C. R_f: 0.33 (CyHex/EtOAc/EtOH, 10:1:1).

Cell Lines and Cultures. The BJAB mock cell line (Burkitt-like lymphoma) was obtained from Prof. Dr. S. Fulda, University of Ulm, Germany. AG Henze, Charité Berlin, Germany provided the Nalm6 (human B-cell precursor leukemia) and HL-60 (human acute myeloid leukemia) cells. 7CCA (doxorubicin-resistant BJAB cells), BiBo (vincristine-resistant BJAB cells), NVCR (vincristine-resistant Nalm6 cells), and NDau (daunorubicin-resistant Nalm6 cells) were generated in our lab by exposing them to increasing concentrations of the mentioned cytostatic drugs. Doxorubicin, vincristine, and daunorubicin were provided by the Children's Hospital Amsterdamer Straße, Cologne, Germany and were freshly dissolved as 40 mM stock solutions in DMSO before use. Compared to the general cell lines, the resistant cells tolerate significant concentrations of the

https://doi.org/10.1021/acsomega.1c04659
ACS Omega 2022, 7, 2591−2603

cytostatic drugs without the loss of vitality. The MCF7 cells are human breast adenocarcinoma cells from Prof. Dr. Reiner Jänicke, University of Düsseldorf, Germany. MCF7(−) cells are caspase-3-deficient, while the modified variant MCF7(+) is capable of caspase-3 expression. The construct MelHO (human melanoma) pIRES/Bcl-2 was provided by Dr. Eberle, Charité, Berlin, Germany. The MelHO-pIRES cells were transfected with the pIRES vector. A modified variant, MelHO-Bcl-2, has the pIRES-Bcl-2 vector included, resulting in strong overexpression of the Bcl-2 protein.[79] Human hepatocytes were obtained from a patient at the Children's Hospital Amsterdamer Straße, Cologne, Germany. Healthy leukocytes were donated by the authors of this paper. All cell lines were incubated in 250 mL cell culture bottles at 37 °C. The RPMI 1640 medium used for suspension cells was obtained from Gibco Invitrogen. Heat-inactivated fetal calf serum (FCS, 10%, v/v), L-glutamine (0.56 g/L), penicillin (100 000 iu), and streptomycin (0.1 g/L) were added. Adherent cells were grown in Dulbecco's modified Eagle's medium (DMEM, GIBCO Invitrogen) supplemented with FCS (10%, v/v) and geniticine (0.4 mg/mL). All cells were passaged 2−3 times per week and diluted to a concentration of 1×10^5 cells/mL. Standard conditions were achieved by adjusting all cells to 3×10^5 cells/mL 24 h before the assay setup. Before pipetting into six-well plates and treating with substances for experiments, cells were diluted to 1×10^5 cells/mL.

Cell Concentration and Viability. A CASY cell counter and analyzer system from Roche was used to measure the cell count and viability with different settings for the cell lines. Cell debris, dead cells, and viable cells were analyzed in one measurement.[68] Cells were seeded at a density of 1×10^5 cells/mL in six-well plates before treating them with different solutions of **7** in DMSO. As the control group, cells were left either untreated or were treated with pure DMSO. The incubation time was 24 h at 37 °C. Then, cells were resuspended and 100 μL of each well was diluted in 10 mL of isotonic saline solution (CASYton) for an immediate automated count of the cells. The control group of the cells was defined as 100% growth.

Cytotoxicity. Cytotoxicity of **7** in BJAB cells was investigated by the lactate dehydrogenase (LDH) release assay. The incubation time was 1 h after treating the cells with the different substances. The release of LDH was measured in the cell culture supernatants by the Cytotoxicity Detection Kit from Roche. Centrifugation at 350*g* for 5 min was followed by diluting 20 μL of cell-free supernatants with 80 μL of phosphate-buffered saline (PBS). About 100 μL of the reaction mixture that contained 2-(4-iodophenyl)-3-(4-nitrophenyl)-5-phenyltetrazolium chloride, sodium lactate, NAD^+, and diaphorase was added. The quantification of time-dependent formation of the reaction product was performed photometrically at 490 nm. As a reference for 100% cell death, control cells were treated with 0.1% Triton X-100.

Apoptosis Differentiation. The Annexin V (V-FITC/PI) (eBioscience) assay was used to differentiate apoptosis states in a BJAB cell culture. The incubation time was 48 h. Then, cells were collected and stained with Annexin V-BITC/PI. Before incubating in the dark at room temperature for 15 min, 5×10^5 cells were resuspended in 50 μL of Annexin V staining buffer (10 mM *N*-(2-hydroxyethyl)piperazine-*N*′-ethanesulfonic acid (HEPES), 140 mM NaCl, and 2.5 mM $CaCl_2$, pH 7.4), and 2.5 μL of Annexin V conjugate and 1.25 μL of PI solution (1 mg/mL) were added. FACSCalibur (Becton Dickinson) and CellQuest Pro (BD) analysis software was used to analyze the signal intensity. For Annexin V-FITC, the excitation and emission settings were 488 nm and 515−545 nm (FL1 channel), respectively, and for PI, these were 564−606 nm (FL2 channel).

DNA Fragmentation. Apoptosis rates were determined by a modified cell cycle analysis, which detects DNA fragmentation on the single-cell level.[69] All cells were pipetted in six-well plates at a density of 1×10^5 cells/mL and then treated with different concentrations of the substances. The incubation time for all cell lines was 72 h at 37 °C except for the human hepatocytes with 96 h of incubation. After that, adherent cells were washed with 180 μL of PBS. After pipetting trypsin on the cells, they were incubated for 5 min at 37 °C. All cells were centrifuged at 6500 rpm for 5 min at 4 °C and then fixed in 200 μL of PBS/2% (v/v) formaldehyde on ice for 30 min. Cells were collected again by centrifugation at 1500 rpm for 5 min at 4 °C and then incubated with 180 μL of ethanol/PBS (2:1, v/v) for 15 min. After centrifugation at 1500 rpm for 5 min at 4 °C, cells were resuspended in 50 μL of PBS containing 40 μg/mL RNase A (Qiagen). RNA was digested for 30 min at 37 °C. Cells were centrifuged again at 1500 rpm for 5 min at 4 °C and then resuspended in 200 μL of PBS containing 50 μg/mL propidium iodide (Serva). Flow cytometric determination of hypodiploid DNA was used to quantify nuclear DNA fragmentation (fluorescence-activated cell sorting, FACS). Using a FACScan by Becton Dickinson, equipped with CELLQuest software, data were collected and analyzed. The percentage of hypoploidy (subG1) reflects the number of apoptotic cells. The induced apoptosis in each concentration of the substances was calculated by subtracting background apoptosis, observed in control cells, from total apoptosis seen in the treated cells.

Immunoblotting. BJAB cells were incubated for 36 h with 5 and 8 nM **7**. Control cells were left untreated. Epirubicin was used as the positive control. Cells were washed twice with PBS and lysed in a buffer containing 10 mM Tris−HCl, pH 7.5, 300 mM NaCl, 1% Triton X-100, 2 mM $MgCl_2$, 5 μM ethylenediamine tetraacetic acid (EDTA), 1 μM pepstatin, 1 μM leupeptin, and 0.1 mM phenylmethylsulfonyl fluoride (PMSF). The bicinchoninic acid assay from Pierce was used to determine the protein concentration.[70] Equal amounts of protein were separated by SDS-PAGE, and immunoblotting was performed as described in the literature.[71,72] Membrane blocking was performed for 1 h in PBST (PBS, 0.05% Tween-20) containing bovine serum albumin (BSA) and followed by incubation with different primary antibodies for 1 h. Anticaspase-3, anticaspase-9, and anti-β-Actin from Sigma, Saint Louis were used. The membrane was washed in PBST, and then, the secondary antibody (antimouse IgG HRP from Bioscience and antirabbit IgG HRP from Promega) was applied for 1 h in PBST. The membrane was washed again. An ECL enhanced chemiluminescence system by Amersham Buchler was used to detect the protein bands.

Mitochondrial Membrane Potential. BJAB cells were treated with different concentrations of **7** for 48 h. After incubation, cells were centrifuged at 300*g* for 5 min at 4 °C and then stained with 5,5′,6,6′-tetrachloro-1,1′,3,3′-tetraethyl-benzimidazolylcarbocyanin iodide (JC-1; Molecular Probes) as described in the literature to measure the mitochondrial permeability transition.[73,74] Cells were then resuspended in 500 μL of phenol-red-free RPMI 1640 without supplements. JC-1 was added (c = 2.5 μg/μL). Cells were then incubated for 30 min at 37 °C while being shaken frequently. Subsequently, cells were collected by centrifugation at 300*g* and 4 °C for 5 min. One sample of control cells was incubated in the absence of JC-1 dye. All cells were washed with ice-cold PBS and resuspended in 200

https://doi.org/10.1021/acsomega.1c04659
ACS Omega 2022, 7, 2591−2603

μL of PBS at 4 °C. The mitochondrial permeability transition was quantified by flow cytometric determination of cells with decreased fluorescence. FACScan was used as described above. Data is given as the percentage of cells with low mitochondrial membrane potential $\Delta\Psi$m.

Microtubule Morphology. Human tumor cell line MDA-MB-231 (triple-negative breast adenocarcinoma) was obtained from the American Type Culture Collection and was cultivated in DMEM (Gibco) supplemented with 10% heat-inactivated fetal calf serum, 100 U/mL penicillin, and 100 μg/mL streptomycin and maintained at 37 °C and 5% CO_2. For microtubule morphology studies, MDA-MB-231 cells were grown to 80% confluency. Treatment with different compounds was carried out for 24 h. Subsequently, the cells were fixed using ice-cold methanol for 10 min followed by 30 min of blocking by treatment with 1 mL of blocking solution (0.5% gelatin from cold-water fish skin in 1× PBS) for 1 h at rt or overnight at 4 °C. The blocked cells could be stored at 4 °C until immunofluorescence staining was carried out. After removal of the blocking solution, the primary antibody was added and incubated for 1 h at rt (CPAP overnight at 4 °C). Some of the primary antibodies were collected back for reuse. After this step, the cells were washed with the blocking solution for an interval of 3 min three times. To add secondary antibodies, the blocking solution was removed and the secondary antibody was added and incubated for 1 h at rt. The same steps were repeated as above for the remaining primary and secondary antibodies, and 4,6-diamidino-2-phenylindole (DAPI) was added with the last used secondary antibody. After the last washing, the blocking solution was removed and distilled H_2O was added. The slides were labeled with cell type, staining, and date. The coverslips were removed from the water and put on paper to dry. Mowiol (8 μL) was applied onto the slide, and the coverslip was placed upside down on top of it. After drying, nail polish was applied to the edges of the coverslip, and the slides were stored in a box at 4 °C until imaging. Images were collected using an Olympus Fluoview FV 1000 scanning confocal microscope. The images were further processed by Fiji and Adobe Photoshop.

X-ray Crystallography. The T_2R complex was obtained by addition of compound **7** to T_2R in a 2.5-fold molar excess over tubulin. Crystals that diffracted X-rays to 2.5 Å resolution were grown in the presence of T_2R seeds obtained from subtilisin-treated tubulin.[75] A complete data set was collected at the Proxima1 beamline (SOLEIL Synchrotron). Data were processed with XDS.[76] Molecular replacement was done with Phaser using 3RYC as the search model.[77] The structural model was refined by BUSTER (Global Phasing Ltd.) with iterative model building in Coot.[78] Figures of structural models were generated with PyMOL (www.pymol.org). For **7** and *rac*-**10**, single-crystal X-ray diffractometry was conducted with suitable crystals (obtained from their respective solutions by solvent evaporation) on a D8 Venture (Bruker) using copper Kα emission (λ = 1.5406 Å) as the measurement radiation. The structural resolution was performed by software SHELXT and refined using SHELXL-2014/7. Images were created by Platon or Schakal99. Data collection and refinement statistics on the respective compounds and the T_2R:**7** complex are listed in the corresponding data sets in the Supporting File.

■ ASSOCIATED CONTENT

Supporting Information

The Supporting Information is available free of charge at https://pubs.acs.org/doi/10.1021/acsomega.1c04659.

^{1}H and ^{13}C NMR spectra and assigned structures for compounds **7**, **9**, *rac*-**10**, and *rac*-**11** as well as X-ray crystallographic data for compounds **7** and *rac*-**10** and the T_2R:**7** complex (PDF)

Accession Codes

The atomic coordinates and structure factors for the T_2R:**7** complex have been deposited in the Protein Data Bank (PDB) under accession code 6TH4.

■ AUTHOR INFORMATION

Corresponding Authors

Aram Prokop − *Department of Paediatric Oncology, Children's Hospital Cologne, 50735 Cologne, Germany; Department of Pediatric Hematology/Oncology, Helios Clinic Schwerin, 19055 Schwerin, Germany; MSH Medical School Hamburg, 20457 Hamburg, Germany*; Email: Aram.Prokop@helios-gesundheit.de

Hans-Günther Schmalz − *Department of Chemistry, University of Cologne, 50939 Cologne, Germany*; orcid.org/0000-0003-0489-1827; Email: schmalz@uni-koeln.de

Authors

Andreas Stein − *Department of Chemistry, University of Cologne, 50939 Cologne, Germany*

Persefoni Hilken née Thomopoulou − *Department of Chemistry, University of Cologne, 50939 Cologne, Germany*

Corazon Frias − *Department of Paediatric Oncology, Children's Hospital Cologne, 50735 Cologne, Germany*

Sina M. Hopff − *Department of Paediatric Oncology, Children's Hospital Cologne, 50735 Cologne, Germany*

Paloma Varela − *Université Paris-Saclay, CEA, CNRS, Institute for Integrative Biology of the Cell (I2BC), 91198 Gif-sur-Yvette cedex, France*; orcid.org/0000-0001-5078-7102

Nicola Wilke − *Department of Paediatric Oncology, Children's Hospital Cologne, 50735 Cologne, Germany*

Arul Mariappan − *Laboratory for Centrosome and Cytoskeleton Biology, Institute of Human Genetics, Heinrich-Heine-University, 40225 Düsseldorf, Germany*

Jörg-Martin Neudörfl − *Department of Chemistry, University of Cologne, 50939 Cologne, Germany*

Alexey Yu Fedorov − *Department of Organic Chemistry, N.I. Lobachevsky State University of Nizhny Novgorod, 603950 Nizhny Novgorod, Russian Federation*; orcid.org/0000-0003-4889-8617

Jay Gopalakrishnan − *Laboratory for Centrosome and Cytoskeleton Biology, Institute of Human Genetics, Heinrich-Heine-University, 40225 Düsseldorf, Germany*

Benoît Gigant − *Université Paris-Saclay, CEA, CNRS, Institute for Integrative Biology of the Cell (I2BC), 91198 Gif-sur-Yvette cedex, France*

Complete contact information is available at: https://pubs.acs.org/10.1021/acsomega.1c04659

Author Contributions

○A.S. and P.H.n.T. contributed equally. The manuscript was written through the contribution of all authors. H.-G.S. and A.P. designed the research; A.S. and P.H.n.T. performed the chemical synthesis and structural elucidation; A.P., C.F., S.M.H., N.W., J.G., and A.M. performed and evaluated biological experiments; B.G., J.-M.N., and P.V. performed X-ray crystallographic measurements and data analyses; A.Y.F. reviewed the

https://doi.org/10.1021/acsomega.1c04659
ACS Omega 2022, 7, 2591−2603

manuscript; and A.S., S.M.H., N.W., and H.-G.S. wrote the paper.

Funding

This work was supported by the Deutsche Forschungsgemeinschaft DFG (SCHM 857/18-1 to H.-G.S.) and the Russian Scientific Foundation (19-13-00158 to A.Y.F.).

Notes

The authors declare no competing financial interest.

■ ACKNOWLEDGMENTS

The authors gratefully acknowledge the Jürgen Manchot foundation (doctoral stipend to P.H.n.T.), Dr. Kleist Stiftung, Berlin (to A.P.), and the "Fondation ARC pour la recherche sur le cancer" (to B.G.). Diffraction data were collected at the Proxima1+2 beamlines at SOLEIL synchrotron (Saint-Aubin, France), and the authors are most grateful to the machine and beamline groups for making these experiments possible.

■ ABBREVIATIONS

BJAB, Burkitt-like lymphoma; CBS, colchicine-binding site; TCI, targeted covalent inhibitor; NCS, *N*-chloro succinimide; Boc, *tert*-butyloxycarbonyl; DMAP, *N*,*N*-dimethylaminopyridine; TFA, trifluoroacetic acid; D^{t}BAD, di-*tert*-butyl azodicarboxylate; DCM, dichloromethane; DIPEA, diisoproylethylamine; DMDO, dimethyldioxirane; AML, acute myeloid leukemia; LDH, lactate dehydrogenase; MDR, multidrug resistance; P-gp, P-gylcoprotein; DMSO, dimethyl sulfoxide; SD, standard deviation; C3, caspase-3; C9, caspase-9; TLC, thin-layer chromatography; PBS, phosphate-buffered saline; PI, propidium iodide; BSA, bovine serum albumin

■ REFERENCES

(1) Graham, W.; Roberts, J. B. Intravenous Colchicine in the Management of Gouty Arthritis. *Ann. Rheum. Dis.* **1953**, *12*, 16−19.
(2) Cocco, G.; Chu, D. C. C.; Pandolfi, S. Colchicine in clinical medicine. A guide for internists. *Eur. J. Intern. Med.* **2010**, *21*, 503−508.
(3) Dalbeth, N.; Lauterio, T. J.; Wolfe, H. W. Mechanism of Action of Colchicine in the Treatment of Gout. *Clin. Ther.* **2014**, *36*, 1465−1479.
(4) Terkeltaub, R. *Gout & Other Crystal Arthropathies*; Saunders: Philadelphia, 2012; pp 187−193.
(5) Raynor, A.; Askari, A. D. Behçet's disease and treatment with colchicine. *J. Am. Acad. Dermatol.* **1980**, *2*, 396−400.
(6) Saleh, Z.; Arayssi, T. Update on the therapy of Behçet disease. *Ther. Adv. Chronic Dis.* **2014**, *5*, 112−134.
(7) Imazio, M.; Gaita, F.; LeWinter, M. Evaluation and treatment of pericarditis: A systematic review. *JAMA* **2015**, *314*, 1498−1506.
(8) Verma, S.; Eikelboom, J. W.; Nidorf, S. M.; Al-Omran, M.; Gupta, N.; Teoh, H.; Friedrich, J. O. Colchicine in cardiac disease: a systematic review and meta-analysis of randomized controlled trials. *BMC Cardiovasc. Disord.* **2015**, *15*, No. 96.
(9) Cerquaglia, C.; Diaco, M.; Nucera, G.; La Regina, M.; Manna, M. M.; Manna, R. Pharmacological and Clinical Basis of Treatment of Familial Mediterranean Fever (FMF) with Colchicine or Analogues: An Update. *Curr. Drug Targets: Inflammation Allergy* **2005**, *4*, 117−124.
(10) Ozen, S.; Demirkaya, E.; Erer, B.; Livneh, A.; Ben-Chetrit, E.; Giancane, G.; Ozdogan, H.; Abu, I.; Gattorno, M.; Hawkins, P. N.; et al. EULAR recommendations for the management of familial Mediterranean fever. *Ann. Rheum. Dis.* **2016**, *75*, 644−651.
(11) Jordan, M. A. Mechanism of Action of Antitumor Drugs that Interact with Microtubules and Tubulin. *Curr. Med. Chem.: Anti-Cancer Agents* **2012**, *2*, 1−17.
(12) Bhattacharyya, B.; Panda, D.; Gupta, S.; Banerjee, M. Antimitotic activity of colchicine and the structural basis for its interaction with tubulin. *Med. Res. Rev.* **2008**, *28*, 155−183.
(13) Gali-Muhtasib, H.; Hmadi, R.; Kareh, M.; Tohme, R.; Darwiche, N. Cell death mechanisms of plant-derived anticancer drugs: beyond apoptosis. *Apoptosis* **2015**, *20*, 1531−1562.
(14) Bornens, M.; Azimzadeh, J. *Origin and Evolution of the Centrosome*; Springer: New York, 2007.
(15) Nogales, E. Structural Insights into Microtubule Function. *Annu. Rev. Biochem.* **2000**, *69*, 277−302.
(16) Schmit, A. C. Acentrosomal Microtubule Nucleation in Higher Plants. In *International Review of Cytology*; Elsevier, 2002; Vol. *220*, pp 257−289.
(17) Ravelli, R. B. G.; Gigant, B.; Curmi, P. A.; Jourdain, I.; Lachkar, S.; Sobel, A.; Knossow, M. Insight into tubulin regulation from a complex with colchicine and a stathmin-like domain. *Nature* **2004**, *428*, 198−202.
(18) Checchi, P. M.; Nettles, J. H.; Zhou, J.; Snyder, J. P.; Joshi, H. C. Microtubule-interacting drugs for cancer treatment. *Trends Pharmacol. Sci.* **2003**, *24*, 361−365.
(19) Mangiatordi, G. F.; Trisciuzzi, D.; Alberga, D.; Denora, N.; Iacobazzi, R. M.; Gadaleta, D.; Catto, M.; Nicolotti, O. Novel chemotypes targeting tubulin at the colchicine binding site and unbiasing P-glycoprotein. *Eur. J. Med. Chem.* **2017**, *139*, 792−803.
(20) Gracheva, I. A.; Shchegravina, E. S.; Schmalz, H.-G.; Beletskaya, I. P.; Fedorov, A. Y. Colchicine Alkaloids and Synthetic Analogues: Current Progress and Perspectives. *J. Med. Chem.* **2020**, *63*, 10618−10651.
(21) Ghawanmeh, A. A.; Chong, K. F.; Sarkar, S. M.; Bakar, M. A.; Othaman, R.; Khalid, R. M. Colchicine prodrugs and codrugs: Chemistry and bioactivities. *Eur. J. Med. Chem.* **2018**, *144*, 229−242.
(22) Kurek, J.; Kwaśniewska-Sip, P.; Myszkowski, K.; Cofta, G.; Murias, M.; Barczyński, P.; Jasiewicz, B.; Kurczab, R. 7-Deacetyl-10-alkylthiocolchicine derivatives − new compounds with potent anticancer and fungicidal activity. *MedChemComm* **2018**, *9*, 1708−1714.
(23) Thomopoulou, P.; Sachs, J.; Teusch, N.; Mariappan, A.; Gopalakrishnan, J.; Schmalz, H.-G. New Colchicine-Derived Triazoles and Their Influence on Cytotoxicity and Microtubule Morphology. *ACS Med. Chem. Lett.* **2016**, *7*, 188−191.
(24) Voitovich, Y. V.; Shegravina, E. S.; Sitnikov, N. S.; Faerman, V. I.; Fokin, V. V.; Schmalz, H.-G.; Combes, S.; Allegro, D.; Barbier, P.; Beletskaya, I. P.; et al. Synthesis and Biological Evaluation of Furanoallocolchicinoids. *J. Med. Chem.* **2015**, *58*, 692−704.
(25) Gracheva, I. A.; Voitovich, I. V.; Faerman, V. I.; Sitnikov, N. S.; Myrsikova, E. V.; Schmalz, H.-G.; Svirshevskaya, E. V.; Fedorov, A. Y. Synthesis and cytostatic properties of polyfunctionalized furanoallocolchicinoids. *Eur. J. Med. Chem.* **2017**, *126*, 432−443.
(26) Gracheva, I. A.; Svirshchevskaya, E. V.; Faerman, V. I.; Beletskaya, I. P.; Fedorov, A. Y. Synthesis and Antiproliferative Properties of Bifunctional Allocolchicine Derivatives. *Synthesis* **2018**, *50*, 2753−2760.
(27) Potashman, M. H.; Duggan, M. E. Covalent Modifiers: An Orthogonal Approach to Drug Design. *J. Med. Chem.* **2009**, *52*, 1231−1246.
(28) Park, B. K.; Boobis, A.; Clarke, S.; Goldring, C. E. P.; Jones, D.; Kenna, J. G.; Lambert, C.; Laverty, H. G.; Naisbitt, D. J.; Nelson, S.; et al. Managing the challenge of chemically reactive metabolites in drug development. *Nat. Rev. Drug Discovery* **2011**, *10*, 292.
(29) Gersch, M.; Kreuzer, J.; Sieber, S. A. Electrophilic natural products and their biological targets. *Nat. Prod. Rep.* **2012**, *29*, 659−682.
(30) Wright, M. H.; Sieber, S. A. Chemical proteomics approaches for identifying the cellular targets of natural products. *Nat. Prod. Rep.* **2016**, *33*, 681−708.
(31) Koch, M. F.; Harteis, S.; Blank, I. D.; Pestel, G.; Tietze, L. F.; Ochsenfeld, C.; Schneider, S.; Sieber, S. A. Structural, Biochemical, and Computational Studies Reveal the Mechanism of Selective Aldehyde Dehydrogenase 1A1 Inhibition by Cytotoxic Duocarmycin Analogues. *Angew. Chem., Int. Ed.* **2015**, *54*, 13550−13554.

https://doi.org/10.1021/acsomega.1c04659
ACS Omega 2022, 7, 2591−2603

(32) Tailor, A.; Waddington, J. C.; Meng, X.; Park, B. K. Mass Spectrometric and Functional Aspects of Drug−Protein Conjugation. *Chem. Res. Toxicol.* **2016**, *29*, 1912−1935.
(33) Liu, T.; Marcinko, T. M.; Kiefer, P. A.; Vachet, R. W. Using Covalent Labeling and Mass Spectrometry To Study Protein Binding Sites of Amyloid Inhibiting Molecules. *Anal. Chem.* **2017**, *89*, 11583−11591.
(34) Lonsdale, R.; Ward, R. A. Structure-based design of targeted covalent inhibitors. *Chem. Soc. Rev.* **2018**, *47*, 3816−3830.
(35) Pettinger, J.; Jones, K.; Cheeseman, M. D. Lysine-Targeting Covalent Inhibitors. *Angew. Chem., Int. Ed.* **2017**, *56*, 15200−15209.
(36) Mukherjee, H.; Grimster, N. P. Beyond cysteine: recent developments in the area of targeted covalent inhibition. *Curr. Opin. Chem. Biol.* **2018**, *44*, 30−38.
(37) Awoonor-Williams, E.; Rowley, C. N. How Reactive are Druggable Cysteines in Protein Kinases? *J. Chem. Inf. Model.* **2018**, *58*, 1935−1946.
(38) Burger, J. A.; Tedeschi, A.; Barr, P. M.; Robak, T.; Owen, C.; Ghia, P.; Bairey, O.; Hillmen, P.; Bartlett, N. L.; Li, J.; et al. Ibrutinib as Initial Therapy for Patients with Chronic Lymphocytic Leukemia. *N. Engl. J. Med.* **2015**, *373*, 2425−2437.
(39) Van Der Steen, N.; Caparello, C.; Rolfo, C.; Pauwels, P.; Peters, G.; Giovannetti, E. New developments in the management of non-small-cell lung cancer, focus on rociletinib: what went wrong? *Onco. Targets. Ther.* **2016**, *9*, 6065−6074.
(40) Awoonor-Williams, E.; Walsh, A. G.; Rowley, C. N. Modeling covalent-modifier drugs. *Biochim. Biophys. Acta, Proteins Proteomics* **2017**, *1865*, 1664−1675.
(41) Bagnato, J. D.; Eilers, A. L.; Horton, R. A.; Grissom, C. B. Synthesis and Characterization of a Cobalamin−Colchicine Conjugate as a Novel Tumor-Targeted Cytotoxin. *J. Org. Chem.* **2004**, *69*, 8987−8996.
(42) Danieli, B.; Lesma, G.; Passarella, D.; Prosperi, D.; Sacchetti, A.; Silvani, A.; Destro, R.; May, E.; Bombardelli, E. New tetracyclic colchicinoids from the reaction of N-deacetylthiocolchicine and N-deacetylcolchicine with nitrous acid and tert-butyl nitrite. *Helv. Chim. Acta* **2003**, *86*, 2082−2089.
(43) Mitsunobu, O.; Yamada, M. Preparation of Esters of Carboxylic and Phosphoric Acid via Quaternary Phosphonium Salts. *Bull. Chem. Soc. Jpn.* **1967**, *40*, 2380−2382.
(44) Sun, L.; McPhail, A. T.; Hamel, E.; Lin, C. M.; Hastie, S. B.; Chang, J. J.; Lee, K. H. Antitumor agents. 139. Synthesis and biological evaluation of thiocolchicine analogs 5,6-dihydro-6(S)-acyloxy)- and 5,6-dihydro-6(S)-[(aroyloxy)methyl]-1,2,3-trimethoxy-9-(methylthio)-8H-cyclohepta[a]naphthalen-8-ones as novel cytotoxic and antimitotic ag. *J. Med. Chem.* **1993**, *36*, 544−551.
(45) Yasobu, N.; Kitajima, M.; Kogure, N.; Shishido, Y.; Matsuzaki, T.; Nagaoka, M.; Takayama, H. Design, Synthesis, and Antitumor Activity of 4-Halocolchicines and Their Pro-drugs Activated by Cathepsin B. *ACS Med. Chem. Lett.* **2011**, *2*, 348−352.
(46) Uderzo, C.; Conter, V.; Dini, G.; Locatelli, F.; Miniero, R.; Tamaro, P. Treatment of Childhood Acute Lymphoblastic Leukemia after the First Relapse: Curative Strategies. *Haematologica* **2001**, *86*, 1−7.
(47) Baguley, B. C. Multidrug Resistance in Cancer. In *Multi-Drug Resistance in Cancer*; Zhou, J., Ed.; Humana Press: Totowa, 2010; pp 1−14.
(48) Kater, L.; Claffey, J.; Hogan, M.; Jesse, P.; Kater, B.; Strauß, S.; Tacke, M.; Prokop, A. The role of the intrinsic FAS pathway in Titanocene Y apoptosis: The mechanism of overcoming multiple drug resistance in malignant leukemia cells. *Toxicol. In Vitro* **2012**, *26*, 119−124.
(49) Gottesman, M. M.; Fojo, T.; Bates, S. E. Multidrug resistance in cancer: role of ATP−dependent transporters. *Nat. Rev. Cancer* **2002**, *2*, 48.
(50) Marques, M. B.; de Oliveira, P. V.; Fagan, S. B.; Oliveira, B. R.; da Silva Nornberg, B. F.; Almeida, D. V.; Marins, L. F.; González-Durruthy, M. Modeling drug-drug interactions of AZD1208 with Vincristine and Daunorubicin on ligand-extrusion binding TMD-domains of multidrug resistance P-glycoprotein (ABCB1). *Toxicology* **2019**, *411*, 81−92.
(51) Qian, J.; Xia, M.; Liu, W.; Li, L.; Yang, J.; Mei, Y.; Meng, Q.; Xie, Y. Glabridin resensitizes p-glycoprotein-overexpressing multidrug-resistant cancer cells to conventional chemotherapeutic agents. *Eur. J. Pharmacol.* **2019**, *852*, 231−243.
(52) Szakács, G.; Paterson, J. K.; Ludwig, J. A.; Booth-Genthe, C.; Gottesman, M. M. Targeting multidrug resistance in cancer. *Nat. Rev. Drug Discovery* **2006**, *5*, 219.
(53) Dawson, R. J. P.; Hollenstein, K.; Locher, K. P. Uptake or extrusion: crystal structures of full ABC transporters suggest a common mechanism. *Mol. Microbiol.* **2007**, *65*, 250−257.
(54) Majno, G.; Joris, I. Apoptosis, oncosis, and necrosis. An overview of cell death. *Am. J. Pathol.* **1995**, *146*, 3−15.
(55) Van Cruchten, S.; Van den Broeck, W. Morphological and Biochemical Aspects of Apoptosis, Oncosis and Necrosis. *Anat., Histol., Embryol.* **2002**, *31*, 214−223.
(56) Jhaveri, A.; Deshpande, P.; Torchilin, V. Stimuli-sensitive nanopreparations for combination cancer therapy. *J. Controlled Release* **2014**, *190*, 352−370.
(57) Nair, P.; Lu, M.; Petersen, S.; Ashkenazi, A. Apoptosis Initiation Through the Cell-Extrinsic Pathway. In *Methods in Enzymology*; Elsevier, 2014; Vol. *544*, pp 99−128.
(58) Herr, I.; Debatin, K.-M. Cellular stress response and apoptosis in cancer therapy. *Blood* **2001**, *98*, 2603−2614.
(59) Lambert, I. H.; Hoffmann, E. K.; Jørgensen, F. Membrane potential, anion and cation conductances in Ehrlich ascites tumor cell. *J. Membr. Biol.* **1989**, *111*, 113−131.
(60) Onambele, L. A.; Koth, D.; Czaplewska, J. A.; Schubert, U. S.; Görls, H.; Yano, S.; Obata, M.; Gottschaldt, M.; Prokop, A. Mitochondrial Mode of Action of a Thymidine-Based Cisplatin Analogue Breaks Resistance in Cancer Cells. *Chem. - Eur. J.* **2010**, *16*, 14498−14505.
(61) Cohen, G. M. Caspases: the executioners of apoptosis. *Biochem. J.* **1997**, *326*, 1−16.
(62) Porter, A. G.; Jänicke, R. U. Emerging roles of caspase-3 in apoptosis. *Cell Death Differ.* **1999**, *6*, 99.
(63) Yang, X.-H.; Sladek, T. L.; Liu, X.; Butler, B. R.; Froelich, C. J.; Thor, A. D. Reconstitution of Caspase 3 Sensitizes MCF-7 Breast Cancer Cells to Doxorubicin- and Etoposide-induced Apoptosis. *Cancer Res.* **2001**, *61*, 348−354.
(64) Youle, R. J.; Strasser, A. The BCL-2 protein family: opposing activities that mediate cell death. *Nat. Rev. Mol. Cell Biol.* **2008**, *9*, 47.
(65) Ahmad, S.; Pecqueur, L.; Dreier, B.; Hamdane, D.; Aumont-Nicaise, M.; Plückthun, A.; Knossow, M.; Gigant, B. Destabilizing an interacting motif strengthens the association of a designed ankyrin repeat protein with tubulin. *Sci. Rep.* **2016**, *6*, No. 28922.
(66) Nicolaus, N.; Zapke, J.; Riesterer, P.; Neudörfl, J.-M.; Prokop, A.; Oschkinat, H.; Schmalz, H.-G. Azides derived from Colchicine and their Use in Library Synthesis: a Practical Entry to New Bioactive Derivatives of an Old Natural Drug. *ChemMedChem* **2010**, *5*, 661−665.
(67) Danieli, B.; Lesma, G.; Passarella, D.; Prosperi, D.; Sacchetti, A.; Silvani, A.; et al. New Tetracyclic Colchicinoids from the Reaction of *N*-Deacetylthiocolchicine and *N*-Deacetylcolchicine with Nitrous Acid and *tert*-Butyl Nitrite. *Helv. Chim. Acta* **2003**, *86*, 2082−2089.
(68) Voisard, R.; Dartsch, P. C.; Seitzer, U.; Roth, D.; Kochs, M.; Hombach, V. Cell culture as a prescreening system for drug prevention of restenosis? *VASA Suppl.* **1991**, *33*, 140−141.
(69) Essmann, F.; Wieder, T.; Otto, A.; Müller, E. C.; Dörken, B.; Daniel, P. T. GDP dissociation inhibitor D4-GDI (Rho-GDI 2), but not the homologous rho-GDI 1, is cleaved by caspase-3 during drug-induced apoptosis. *Biochem. J.* **2000**, *346*, 777−783.
(70) Smith, P. K.; Krohn, R. I.; Hermanson, G. T.; Mallia, A. K.; Gartner, F. H.; Provenzano, M. D.; Fujimoto, E. K.; Goeke, N. M.; Olson, B. J.; Klenk, D. C. Measurement of protein using bicinchoninic acid. *Anal. Biochem.* **1985**, *150*, 76−85.
(71) Laemmli, U. K. Cleavage of structural proteins during the assembly of the head of bacteriophage T4. *Nature* **1970**, *227*, 680−685.

https://doi.org/10.1021/acsomega.1c04659
ACS Omega 2022, 7, 2591−2603

(72) Wieder, T.; Geilen, C. C.; Wieprecht, M.; Becker, A.; Orfanos, C. E. Identification of a putative membrane-interacting domain of CTP: Phosphocholine cytidylyltransferase from rat liver. *FEBS Lett.* **1994**, *345*, 207−210.
(73) Lambert, I. H.; Hoffmann, E. K.; Jørgensen, F. Membrane potential, anion and cation conductances in Ehrlich ascites tumor cell. *J. Membr. Biol.* **1989**, *111*, 113−131.
(74) Reers, M.; Smiley, S. T.; Mottola-Hartshorn, C.; Chen, A.; Lin, M.; Chen, L. B. Mitochondrial Membrane Potential Monitored by JC-1 Dye. In *Methods in Enzymology*; Attardi, G. M.; Chomyn, A., Eds.; Academic Press: Cambridge, 1995; Vol. *260*, pp 406−417.
(75) Nawrotek, A.; Knossow, M.; Gigant, B. The Determinants That Govern Microtubule Assembly from the Atomic Structure of GTP-Tubulin. *J. Mol. Biol.* **2011**, *412*, 35−42.
(76) Kabsch, W. XDS. *Acta Crystallogr., Sect. D: Biol. Crystallogr.* **2010**, *66*, 125−132.
(77) McCoy, A. J.; Grosse-Kunstleve, R. W.; Adams, P. D.; Winn, M. D.; Storoni, L. C.; Read, R. J. Phaser crystallographic software. *J. Appl. Crystallogr.* **2007**, *40*, 658−674.
(78) Emsley, P.; Lohkamp, B.; Scott, W. G.; Cowtan, K. Features and development of Coot. *Acta Crystallogr., Sect. D: Biol. Crystallogr.* **2010**, *66*, 486−501.
(79) Jesse, P.; Mottke, G.; Eberle, J.; Seifert, G.; Henze, G.; Prokop, A. Apoptosis-Inducing Activity of Helleborus niger in ALL and AML. *Pediatr. Blood Cancer* **2009**, 464−469.

https://doi.org/10.1021/acsomega.1c04659
ACS Omega 2022, 7, 2591−2603